

# Chemical compositions of stars in two stellar streams from the Galactic thick disk

P. Ramya,<sup>1\*</sup> Bacham E. Reddy<sup>1</sup> and David L. Lambert<sup>2</sup>

<sup>1</sup>*Indian Institute of Astrophysics, Bengaluru, India-560034*

<sup>2</sup>*University of Texas, McDonald Observatory, Austin, TX, USA*

4 July 2012

## ABSTRACT

We present abundances for 20 elements for stars in two stellar streams identified by Arifyanto & Fuchs 2006: 18 stars from the Arcturus stream and 26 from a new stream, which we call AF06 stream, both from the Galactic thick disk. Results show both streams are metal-poor and very old (10–14 Gyrs) with kinematics and abundances overlapping with the properties of local field thick disk stars. Both streams exhibit a range in metallicity but with relative elemental abundances that are identical to those of thick disk stars of the same metallicity. These results show that neither stream can result from dissolution of an open cluster. It is highly unlikely that either stream represents tidal debris from an accreted satellite galaxy. Both streams most probably owe their origin to dynamical perturbations within the Galaxy.

**Key words:** stars: abundances — stars: moving groups— Galaxy: kinematics and dynamics—Galaxy: disk

## 1 INTRODUCTION

The phase space of the Galaxy’s disk, as observed near the Sun, contains substructure within the larger structures known as the thin and the thick disk. Substructures include open clusters and stellar streams, also often referred to as moving groups. Moving groups, as promoted by Eggen (see e.g., Eggen 1998 and references therein), are considered to be stars having a common space motion and a common chemical composition, and originating from a dissolving open cluster. While some of the well known moving groups do share a common composition (e.g., the HR 1614 group - De Silva et al. 2007) suggesting they come from a tidally-disrupted open cluster, other groups contain stars having very different compositions, a result demanding an origin more complex than disruption of an open cluster. The term ‘stream’ is now applied to some entities in Galactic phase space. Examples in the thin disk include the Hercules stream (Bensby et al. 2007) and the Hyades stream or supercluster (De Silva et al. 2011, Pompéia et al. 2011). For streams in the thin disk, a likely explanation involves dynamical interactions of disk stars with the central bar (Antoja et al. 2009) or spiral density waves (Minchev et al. 2010). Other possibilities arise for streams belonging to the thick disk including accretion from external galaxies.

In this paper, we present chemical compositions for subdwarfs belonging to two streams in the thick disk.

Arifyanto & Fuchs (2006) undertook a search for fine structure in the phase space populated by subdwarfs from the large sample of F and G subdwarfs considered by Carney et al. (1994) for which Arifyanto & Fuchs (2006) refined data on stellar distances and kinematics. Two clumps in phase space were noted by Arifyanto & Fuchs (2006). One with  $V = -125 \text{ km s}^{-1}$  and  $\sqrt{U^2 + 2V^2} = 185 \text{ km s}^{-1}$  is referred to as the Arcturus stream. An Arcturus moving group had been previously identified by Eggen (1971). The second stream AF06 with a stronger presence in phase space than the Arcturus stream is at  $V = -80 \text{ km s}^{-1}$  and  $\sqrt{U^2 + 2V^2} = 130 \text{ km s}^{-1}$ .

Here, we report chemical compositions of stars from these two streams. We show that stars in both streams span a range in metallicity but with relative abundances which match closely the ratios reported for field thick disk stars. This result serves to constrain greatly explanations for the origins of the two streams.

## 2 SAMPLES STARS AND OBSERVATIONS

Stars selected for observation came from membership lists of the Arcturus and AF06 streams given by Arifyanto & Fuchs (2006): 18 of the 22 stars in former stream and 26 of the 44 stars in the latter stream were observed successfully with the Tull coude spectrograph (Tull et al. 1995) at the 2.7 meter Harlan J. Smith telescope of the W.J. McDonald Observatory.

\* E-mail: ramyap@iiap.res.in

Spectra at a resolving power of 60,000 were obtained with spectral coverage from about 3800 Å - 10000 Å with echelle orders incompletely recorded on the CCD beyond about 5800 Å. Wavelength calibration was provided by an exposure of a Th-Ar hollow cathode lamp. These two-dimensional data were reduced to one-dimensional relative flux versus wavelength spectra using the Image Reduction and Analysis Facility <sup>1</sup>(IRAF). In a typical spectrum, the S/N ratio at the centre of an order over most of the full spectral range was 100 or greater.

### 3 ANALYSIS

#### 3.1 Stellar Atmospheric Parameters

Atmospheric parameters – effective temperature ( $T_{\text{eff}}$ ), surface gravity ( $\log g$ ) and metallicity ( $[M/H]$ ) have been derived from both photometric and spectroscopic data. In the former case, we relied on published catalogues of photometry and parallaxes, empirical calibrations and the theoretical stellar evolutionary models. And, in the latter case, our high resolution spectra were used to derive the atmospheric parameters including microturbulence ( $\xi_t$ ). Below, both the procedures are described in brief.

##### 3.1.1 Photometry

The  $T_{\text{eff}}$  is derived using (V- $K_s$ ) colour and Strömgren photometry (*uvby*) calibrations. The  $K_s$  magnitude is taken from 2MASS catalogue<sup>2</sup> (Cutri et al. 2003). The subscript "s" stands for the bandpass of the K filter in the 2MASS survey, i.e., the  $K_s$  filter is narrower than the Johnson K filter. The  $K_s$  magnitudes are converted to standard "K" magnitudes using relations given in Ramírez & Meléndez (2005). The mean difference between the two magnitudes is only  $K_s - K_{\text{tes}} = -0.001 \pm 0.005$  and will have no effect when  $K_s$  is used in place of K magnitudes in the calibration between (V-K) and  $T_{\text{eff}}$ . The V magnitudes for all the stars were adopted from Kharchenko (2001). The (V-K) colour and the empirical relations provided in Alonso et al. (1996) are used in deriving  $T_{\text{eff}}$ . Strömgren colours and indices ( $b-y$ ,  $m_1$ ,  $c_1$ ) are available for 26 out of 44 stars in the sample (Hauck & Mermilliod 1998). Values of metallicity and  $T_{\text{eff}}$  were obtained using empirical calibrations of Strömgren colours and indices given in Schuster & Nissen (1989) and Alonso et al. (1996), respectively. Values of metallicity are quite sensitive to reddening as it makes observed ( $b-y$ ) more positive and  $m_1$  values more negative than their intrinsic colours. However, we expect no significant reddening as the stars are nearby ( $d < 130$  pc from the Sun). Using the methods given in Schuster & Nissen (1989), reddening

values  $E(b-y)$  have been estimated and, indeed, all reddening estimates are vanishingly small:  $E(b-y) \leq 0.001 \pm 0.006$ . Temperatures derived using (V- $K_s$ ) and Strömgren colours are given in Table 1 as  $(T_{\text{eff}})_{V-K}$  and  $(T_{\text{eff}})_{b-y}$ , respectively. The mean difference between the two temperatures,  $(T_{\text{eff}})_{V-K} - (T_{\text{eff}})_{b-y} = 18 \pm 90$  K, excluding the outliers HIP24030, HIP53070, HIP11952 and G192-21, for which the difference is large  $245 \pm 24$  K, i.e.,  $T_{\text{eff}}$  derived from (V- $K_s$ ) colour are hotter than those from ( $b-y$ ). The ( $b-y$ ) temperature of HIP 24030 and (V- $K_s$ ) temperature of G192-21 are much closer to the values obtained using spectroscopy. In the case of the other two, we suspect errors in one of the their colours.

The  $\log g$  value is derived from the trigonometrical parallax, the (B-V) colour, and theoretical isochrones (Demarque et al. 2004). Errors in the parallax and (B-V) colour are taken into account in estimating the uncertainty in the  $\log g$  value.

##### 3.1.2 Spectroscopy

A full set of atmospheric parameters ( $T_{\text{eff}}$ ,  $\log g$ ,  $\xi_t$ ,  $[M/H]$ ) has been derived from spectral line analysis by standard LTE techniques. In this exercise, the LTE Kurucz grid of ATLAS9 model atmospheres with the convective overshoot option was adopted (Kurucz 1998). The rationale for choosing overshoot models for solar type dwarf stars was given in Reddy et al. (2003, 2006). Since we intend to compare our results with the results from the thin and thick disk studies of Reddy et al., we followed their analysis techniques. The LTE line analysis code MOOG (Sneden 1973) in its 2009 version was used throughout.

The effective temperature was set by the requirement that the Fe abundance provided by Fe I lines be independent of the lower excitation potential (LEP) of the selected lines. While deriving  $T_{\text{eff}}$ , caution was taken to minimise the effect of microturbulence by choosing, initially, very weak lines with a sufficient range in LEP. Later, microturbulence ( $\xi_t$ ) was derived by adding Fe I lines of moderately strong equivalent width ( $W_\lambda \leq 120$  mÅ) so that the abundance trend becomes sensitive to changes in  $\xi_t$ . The chosen value of  $\xi_t$  is that for which the abundance is independent of equivalent width. The surface gravity  $\log g$  was obtained by requiring that, for the given  $T_{\text{eff}}$  and  $\xi_t$ , Fe I and Fe II lines give the same Fe abundance. The uncertainties in the derived parameters have been estimated by inspection of dependencies for combinations of models of different sets of parameters. In the case of  $T_{\text{eff}}$ , we varied the best representative  $T_{\text{eff}}$  in steps of 25 K for given  $\log g$ ,  $\xi_t$  and  $[M/H]$ . For steps of 25 K changes, we found no significant changes in the slope as well as in abundances, however, we see (See Figure 2) noticeable changes in abundance trends by increasing or decreasing 50 K from its mean model  $T_{\text{eff}}$ . Thus, we estimate  $\pm 50$  K as an uncertainty in the best fit model atmosphere. Similarly, we found model uncertainties in  $\log g$  and  $\xi_t$ . In Figure 2, estimation of uncertainties is illustrated for  $T_{\text{eff}}$  and  $\xi_t$ . In this way, we found model uncertainties in  $T_{\text{eff}}$ ,  $\log g$ , and  $\xi_t$ :  $\pm 50$  K,  $\pm 0.20$  cm s<sup>-2</sup>,  $\pm 0.20$  km s<sup>-1</sup>, respectively. These individual uncertainties translate to an effective error of  $\pm 0.05$  dex in metallicity  $[Fe/H]$ .

Next, photometric and spectroscopic estimates of model atmosphere parameters are compared. Temperature,  $\log g$

<sup>1</sup> IRAF is distributed by the National Optical Astronomy Observatory, which is operated by the Association of Universities for Research in Astronomy (AURA) under cooperative agreement with the National Science Foundation.

<sup>2</sup> This publication makes use of data products from the 2MASS, which is a joint project of the University of Massachusetts and the Infrared Processing and Analysis Centre/California Institute of Technology, funded by the National Aeronautics and Space Administration (NASA) and the National Science Foundation

and metallicity comparisons are given in Figure 1. The mean difference between  $(T_{\text{eff}})_{V-K}$  and spectroscopic  $T_{\text{eff}}$  is just  $-9 \pm 87$  K. There are a few outliers HIP24030 and HIP94931 (for which  $(T_{\text{eff}})_{b-y}$  values are closer to spectroscopic  $T_{\text{eff}}$ ), G10-12 and HIP9080 (for which  $(T_{\text{eff}})_{b-y}$  not available) with a difference of  $-77 \pm 174$  K. Excluding the outliers the mean difference becomes  $-2 \pm 73$  K. The  $\log g$  values obtained from photometry are in good agreement with the spectroscopic values: the difference between the two methods is only  $0.002 \pm 0.18 \text{ cm s}^{-2}$  for 23 stars for which photometric gravities could be obtained, a difference within the combined uncertainties. The mean difference between the photometric metallicity from Strömgren photometry and the spectroscopic metallicity is  $-0.03 \pm 0.11$  dex for 25 stars for which Strömgren photometry is available. Star G192-21 is an outliers whose spectroscopic metallicity is about 0.7 dex metal richer compared to the corresponding photometric value. Difference is probably due to erroneous Strömgren photometry. For the two metal-poor stars HIP53070 and HIP11952, too few lines are available for a spectroscopic determination of parameters and, therefore, we have adopted photometric  $(T_{\text{eff}})_{b-y}$  and  $\log g$  values. The microturbulent velocity  $\xi_t$  calculated using the relation given in Reddy et al. (2003) between  $\xi_t$ ,  $T_{\text{eff}}$ , and  $\log g$  was adopted for both stars. In the final calculations of abundances we adopt parameters derived from spectroscopy but no conclusions would be changed were the photometric parameters adopted.

### 3.2 Abundances

Elemental abundances have been derived using measured equivalent widths and synthetic spectra with LTE model atmospheres for the adopted stellar parameters taken from Kurucz grid (Kurucz 1998) and the 2009 version of LTE line analysis code MOOG. The line list compiled by Reddy et al. (2006) was adopted. Solar abundances derived by Reddy et al. (2003) have been used as reference values, except Eu abundance. The solar Eu abundance ( $\log \varepsilon(\text{Eu}) = 0.55$ ) has been derived, for this study, using the Atlas solar spectrum (Hinkle et al. 2000) and two Eu II lines (6645.13 Å, 4129.72 Å). For transitions with significant hyperfine structure (HFS) data were taken from Kurucz HFS data base (Kurucz 1998). The lines of Mn, V, Cu, and Eu with HFS were analyzed by computing synthetic spectra. In the case of vanadium, the line at 6216.36 Å, one of the six lines used previously, is now judged to be blended in the cooler stars and is omitted from the analysis of such stars. Elemental abundances are summarized in Tables 2 and 3.

Uncertainties in the derived abundances arise primarily from uncertainties in the derived atmospheric parameters, the equivalent widths ( $W_\lambda$ ) and oscillator strengths ( $\log gf$ ). The latter two quantities affect primarily the line-to-line scatter. Of course, the line-to-line scatter is to some extent also influenced by uncertain model parameters. Uncertainty in the  $\log gf$  values is minimized as our analysis is a differential one with respect to solar spectrum and photospheric abundances. Error in the measured  $W_\lambda$  is estimated following the recipe given in Cayrel (1988). For the quality of our data, uncertainty in the measured  $W_\lambda$  varies from 1mÅ to about 2.5mÅ. We have taken on average 2mÅ as the uncertainty in the measured  $W_\lambda$ . In Table 4, we have provided for one representative star (HIP40613), estimated

uncertainties for each element in the form of  $\Delta[X/\text{Fe}]$  due to  $\delta T_{\text{eff}}$ ,  $\delta \log g$ ,  $\delta \xi_t$ ,  $\delta[M/\text{H}]$ , and  $\delta W_\lambda$ . Assuming all five sources of error discussed above are independent, the combined error is obtained by adding them in quadrature. This we call our measured uncertainty or  $\sigma_{\text{model}}$ .

Uncertainties in abundances can also be gauged by comparing results for stars that are common in this and other studies. For seven stars that are common with thick disk sample study by Reddy et al. (2006), differences in the derived abundance ratios  $[X/\text{Fe}]$  between the studies are given in Table 5. The differences are quite small and less than measured uncertainty ( $\sigma_{\text{model}}$ ). The good agreement between the two studies implies that the results of the two streams in this study can be compared directly with the results of thick disk sample study from Reddy et al. (2006). This is akin to a differential analysis with respect to thick disk.

### 3.3 Kinematics

Both streams were identified by Arifanto & Fuchs (2006) as over-densities of stars in phase space. To represent stars in phase space one requires information such as coordinates, radial velocities, distance (parallaxes), and proper motions. In the calculation of Galactic motions Arifanto & Fuchs (2006) used Hipparcos data (Perryman et al. 1997) and radial velocities from Carney et al. (1994). Recently, Hipparcos observations were re-reduced by van Leeuwen (2007). Consequently, we have rederived the Galactic velocities ( $U$ ,  $V$ ,  $W$ ) for stream members using the revised Hipparcos parallaxes and proper motions and including the radial velocities derived from our McDonald spectra. Radial velocities obtained in this study are in very good agreement with the velocities given in Arifanto & Fuchs (2006). The mean difference between the two studies is  $0.15 \pm 0.50 \text{ km s}^{-1}$ .

The  $U$ ,  $V$  and  $W$  velocities with respect to the Sun were calculated using the method given in Johnson & Soderblom (1987). A right-handed coordinate system is used throughout where  $U$  is positive towards the Galactic center,  $V$  is positive in the direction of Galactic rotation and  $W$  is positive towards the North Galactic Pole (NGP). Velocities ( $U$ ,  $V$ ,  $W$ ) are in good agreement with values given by Arifanto & Fuchs (2006); differences between the two studies are mainly due to the updated parallaxes. None of the stars identified as members by Arifanto & Fuchs (2006) lost their membership in either stream. Derived radial velocities ( $R_v$ ) and Galactic velocities ( $U_{\text{LSR}}$ ,  $V_{\text{LSR}}$ ,  $W_{\text{LSR}}$ ) relative to Local Standard of Rest (LSR) are given in Table 6. In conversion to the LSR frame, the solar motion of ( $U_\odot$ ,  $V_\odot$ ,  $W_\odot$ ) = (+10.0, +5.3, +7.2)  $\text{km s}^{-1}$  is used (Dehnen & Binney 1998).

The mean motion ( $U_{\text{LSR}}$ ,  $V_{\text{LSR}}$ ,  $W_{\text{LSR}}$ ) of the Arcturus stream based on the 18 member stars observed by us is  $(-6.48 \pm 49.29, -124.79 \pm 8.92, -11.5 \pm 49.59)$  and for AF06 stream the mean motion is  $(-41.55 \pm 47.45, -87.35 \pm 7.83, 3.82 \pm 54.34)$ . These values are in good agreement with the streams' central values given in Arifanto & Fuchs (2006).

To compute orbital parameters, the ( $U$ ,  $V$ ,  $W$ ) of each star is integrated over the Galactic potential provided by D. Lin (private communication). Orbital parameters: mean of apogalactic and perigalactic distance ( $R_m$ ), eccentricity ( $e$ ), maximum distance star away from the Galactic plane

( $Z_{\max}$ ) have been derived and given in Table 6. A distance of 8.5 kpc between the Sun and the Galactic center is used in the calculation.

The (U,V,W) of both the streams, as Arifyanto & Fuchs (2006) appreciated, suggest that the streams are part of the thick disk. Probabilities that a particular star belongs to the halo, the thick or the thin disk are calculated using the definitions and recipes given in Reddy et al. (2006). The percentage probability (P) that a star belongs to the thick disk is given in Table 6. All the Arcturus stream members in our sample are thick disk stars with a probability  $P_{\text{Thick}} \geq 80\%$ , while 15 out of the 26 AF06 stream members have a probability that would qualify them as thick disk members with the remaining 11 stars having probabilities placing them in either the thin or thick disks.

In Figure 3, sample stars of the two streams along with the representative members of the thick disk, the thin disk and the halo are shown in the space of angular momentum per unit mass components  $J_z$ , and  $J_{\perp} = \sqrt{J_x^2 + J_y^2}$  the azimuthal and perpendicular components, respectively. In angular momentum space, stars are clustered in a small region compared to their distribution in the velocity space (see Helmi & Zeeuw (2000)). Values are calculated in the right-handed coordinate system and the LSR velocity is assumed to be  $220 \text{ km s}^{-1}$ . The value  $J_z = 0$  implies no rotational velocity in the direction of the Galactic rotation and increasing values mean higher rotational velocities. The  $J_{\perp}$  represents extent of tilt of star's orbit with respect to the Galactic plane. Obviously, for the thin disk it is quite small. Arcturus stream and AF06 stream have a mean  $J_z$  of  $-811 \pm 77 \text{ kpc km s}^{-1}$  and  $-1130 \pm 63 \text{ kpc km, s}^{-1}$ , respectively.

The presence of the Arcturus stream was detected by Navarro et al. (2004) in catalogues of metal-poor stars by Beers et al. (2000) and Gratton et al. (2003). They found the Arcturus stream lagging the LSR by  $120 \text{ km s}^{-1}$  but with a large dispersion of  $\sigma_V \sim 50 \text{ km/s}$ . Their detected structure has angular momentum ( $J_z$ ) in the range of  $(700 - 1100) \text{ km s}^{-1} \text{ kpc}$ . It appears to us that this structure detected by Navarro et al. (2004) is the combined structure of the Arcturus and the AF06 stream but this structure was separated into two different streams by Arifyanto & Fuchs (2006) using the wavelet transform technique. By combining our samples of both streams, we get mean values  $V_{\text{LSR}}$  and  $J_z$  ( $-102.67 \pm 20.34$ ,  $-1000 \pm 173$ ) very similar to what Navarro et al. (2004) found for the structure that they thought to be the single structure labelled the Arcturus stream. The Arcturus stream has been identified in recent studies (Klement et al. 2008) as a significant over density in phase space. Klement et al. (2008)'s study is based on more than 7000 stars within a distance of 500 pc taken from RAVE survey. They have identified stars with high orbital eccentricities having over-densities at about  $V = -120 \text{ km s}^{-1}$  and the second one at  $V = -95 \text{ km s}^{-1}$  which coincide with phase space coordinates of the Arcturus and AF06 streams as given Arifyanto & Fuchs (2006). Williams et al. (2009) examined a data set of 16,000 giants from the RAVE survey and showed pronounced over-density of stars at velocities overlapping with the Arcturus stream in the solar circle.

### 3.4 Ages

Determination of stellar ages from location of a star in a colour-magnitude diagram is an uncertain procedure because the majority of the stars in both streams fall very close to the zero age main sequence. For the few stars that appear relatively evolved off the main sequence ages were estimated. Mean ages with upper and lower limits are given in Table 6. Errors in B-V and parallaxes are used to estimate the limits. In Figure 4, the stars are shown in the HR diagram of  $M_V$  versus (B-V) colour along with isochrones of ages 10 Gyrs, 12 Gyrs and 16 Gyrs for the metallicities  $[\text{Fe}/\text{H}] = -0.70$  dex and  $[\text{Fe}/\text{H}] = -0.51$  dex, for Arcturus stream and AF06 stream respectively. Ages of the stream members range from 10 to 14 Gyrs. The stellar ages, therefore, are very similar to the ages of thick disk field stars which are all older than about 10–11 Gyr (Reddy et al. 2006). The derived ages are in good agreement with previous studies of Arcturus group (cf. Williams et al. 2009, Helmi et al. 2006, Navarro et al. 2004) based on different selections of stream members.

## 4 RESULTS AND DISCUSSION

### 4.1 Chemical signatures

Since their discovery (cf. Eggen 1957), various theories have been put forward to explain the substructures in phase space known variously as moving groups or stellar streams. The most prominent theories identify a stellar stream as either a) a dissolved open cluster, b) debris from an accreted satellite galaxy, or c) the result of dynamical perturbations within the Galaxy.

In establishing the correct explanation for a particular stream, the importance of the chemical signatures or chemical tagging of stream members has been recognized (Freeman & Bland-Hawthorn 2002, Bensby et al. 2007, Williams et al. 2009, De Silva et al. 2007) not only to pinpoint their origin but also to understand the formation and evolution of the disk.

Quantitative abundances of twenty elements has been extracted here for members of the two streams. There are three main groups of elements: iron peak (V, Cr, Mn, Fe, Ni, Co),  $\alpha$ -elements (O, Mg, Si, Ca, Ti), and heavy elements such as  $s$ -process (Ba, Nd) and  $r$ -process (Eu) elements. For the present (thin) disk, iron peak elements mostly come from Type Ia supernovae explosions (SNIa) and the  $\alpha$ -elements are primarily produced in Type II supernovae (SNII). The  $s$ -process elements are known to be produced mainly in evolved stars of low and intermediate mass ( $1 - 8 M_{\odot}$ ) with the lighter  $s$ -process elements also contributed by SNII. Eu, an  $r$ -process element, is most probably produced in SNII. Therefore, an abundance ratio of products of SNIa and SNII helps to track the chemical history of a stellar system.

Abundances of elements from O to Eu in the form of  $[X/\text{Fe}]$  ratios, where X is any element, are given in Table 2 and 3 and shown in Figures 5, 6, and 7 as the run of  $[X/\text{Fe}]$  against  $[\text{Fe}/\text{H}]$ . The metallicity distribution of the streams is shown in Figure 8 for the Arcturus and AF06 streams. Next, we discuss these abundances for the Arcturus and AF06 streams in the light of the proposed scenarios for the origin of stellar streams.

## 4.2 Dissolved Stellar Clusters

Dispersal of an open cluster as the origin of a stellar stream is one explanation from the suite of potential explanations that is directly testable from photometric and spectroscopic determinations of stellar compositions. Given that open clusters exhibit chemical homogeneity, if a stream represents a dissolved cluster, one requires chemical homogeneity also among stream members.

Chemical homogeneity is not a characteristic of these two streams. Results shown in Figure 8 and Table 2 show that stellar metallicities span a wide range for both streams. For the Arcturus stream,  $[\text{Fe}/\text{H}]$  runs from  $-1.40$  to  $-0.37$ . For AF06 stream, the range is from  $-1.69$  to  $+0.22$  but the range is  $-1.69$  to  $-0.17$  for those 15 members with a high probability of belonging to the thick disk. For a strictly homogenous populations such as open and globular clusters the degree of chemical homogeneity is quite high and which is about 0.05 dex (De Silva et al. 2006, Pancino et al. 2010) for a number of elements. In the case of  $[\text{Fe}/\text{H}]$  dispersions are found to be in the range of 0.02 – 0.1 and in some extreme cases dispersions are of the order of 0.2 dex (Paunzen et al. 2010). The wide range in metallicity clearly shows that the systems from which the stream members originated had a relatively long history with a multiple episodes of star formation.

We have also inspected the sample for an evidence of a sub-group with chemical homogeneity. Results shown in Figure 5, 6 and 7 indicate existence of no such a group among Arcturus stream sample, however, for the stream AF06, we find a hint of clustering of stars at  $[\text{Fe}/\text{H}] = -0.4$ . About 8 stars (out of total 26) show metallicity  $[\text{Fe}/\text{H}] = -0.4$  within the dispersion of 0.04 dex. Does it mean that part of the sample stars originated from the disrupted cluster? Probably not, this may be a manifestation of thick disk metallicity distribution which peaks at about  $-0.6$  dex, and to some extent due to a smaller sample size. Thus, neither the Arcturus nor the AF06 stream, as shown by metallicity distribution of member stars of the two streams (see Figure 8), is a dissolved open cluster. This conclusion about the Arcturus stream was reached also by Williams et al. (2009) who selected 134 stream members by selection criteria different from those used by Arifanto & Fuchs (2006) and applied to stellar catalogues other than that compiled by Carney et al. (1994). Their analyses of high-resolution spectra led to a  $[\text{Fe}/\text{H}]$  range similar to that quoted above (see also Navarro et al. (2004)).

## 4.3 Are the streams chemically identical to thick disk field stars?

Among thick disk field stars in the solar neighborhood, there is a strikingly very small dispersion in elemental abundance ratios, i.e.,  $[\text{X}/\text{Fe}]$  at a given  $[\text{Fe}/\text{H}]$ . Indeed, Reddy et al. (2006) found the  $[\text{X}/\text{Fe}]$  to be Gaussian-like with a dispersion  $\sigma$  of less than 0.10 dex for the most of the elements except for V, Y, and Zr for which  $\sigma$  is slightly more than 0.1 dex. Furthermore, such dispersions were uncorrected for measurement uncertainties so that the intrinsic or ‘cosmic’ dispersion must be very small.

In sharp contrast to the very similar  $[\text{X}/\text{Fe}]$  ratios at a given  $[\text{Fe}/\text{H}]$  for local field stars, element ratios reflecting

different contributions from major processes of stellar nucleosynthesis do vary from stellar system to stellar system. For example, ratios in the Galactic bulge are not uniformly identical at a given  $[\text{Fe}/\text{H}]$  to those among local thick or thin disk field stars. Similarly, ratios of  $\alpha$ -elements ( $[\alpha/\text{Fe}]$ ) at a given  $[\text{Fe}/\text{H}]$  among stars of dwarf spheroidal galaxies differ appreciably from those of local stars and from galaxy to galaxy (Venn et al. 2004, Tolstoy et al. 2009, Kirby 2011). This has been illustrated in Figure 9 where ratio of  $[\alpha\text{-process}/\text{Fe}]$  (mean of  $\alpha$ -process elements Mg, Si, Ca and Ti) is compared with that of thick disk (Reddy et al. 2006) and a number of dwarf spheroidal galaxies for which data was taken from (Venn et al. 2004, Monaco et al. 2005).

Therefore, the chemical signatures or tags in the form of  $[\text{X}/\text{Fe}]$  for those key elements from the major processes of nucleosynthesis may test some proposed origins for the streams. To address the question ‘Are these two streams chemically identical to thick disk field stars?’, we show plots of  $[\text{X}/\text{Fe}]$  versus  $[\text{Fe}/\text{H}]$  in Figures 5 to 7 with field stars from Reddy et al. (2006) shown as by grey symbols, and the Arcturus and AF06 stream members shown as black filled circles. To quantify possible systematic offsets between the field thick disk and stream members, we compute mean values and dispersions for the Arcturus and AF06 streams over the  $[\text{Fe}/\text{H}]$  interval  $-0.30$  to  $-1.0$ . Dispersions about the trends is a combination of both the cosmic scatter as well as errors associated with the model parameters. The values ( $\sigma_{\text{AF06}}$ ,  $\sigma_{\text{Arcturus}}$ ) are computed as the standard deviation of the residuals from straight line fits to abundance trends of  $[\text{X}/\text{Fe}]$  against  $[\text{Fe}/\text{H}]$ . Similarly,  $\sigma_{\text{Thickdisk}}$  for the thick disk abundance trends of Reddy et al. (2006) are computed over the same interval. All results are provided in Table 7. In Figure 10, we made comparison of  $\sigma_{\text{Thickdisk}}$  with those of Arcturus and AF06 streams. Dispersion values about the abundance trends of Arcturus stream show very good agreement with that of the thick disk within about 0.02. However, for AF06 stream, in most cases, dispersions are lower by 0.01 – 0.03 compared to thick disk dispersions. With the current limited sample it would be far fetching to attribute this to the different chemical evolution for the AF06 stream and hence external origin to it. Mean abundances of Arcturus and AF06 streams are quite similar and the differences are within 0.05 dex except three elements (O, Cu, Eu) for which difference is 0.06 - 0.07 dex. Dispersions about the trends for all the elements are comparable to the estimated scatter ( $\sigma_{\text{model}}$ ) due to uncertainties in model parameters. Differences between dispersions and  $\sigma_{\text{model}}$  are within 0.05 dex. Thus, we conclude that the streams are chemically identical to within high precision with the field thick disk stars. Given that external galaxies of the Local Group have different element ratios across the  $[\text{Fe}/\text{H}]$  range sampled by these two streams, especially for  $\alpha$ -elements (see, for example, Tolstoy et al. (2009), Figure 11), it seems most unlikely that either stream represents debris from an accreted satellite galaxy.

## 5 CONCLUSIONS

The outstanding results of our abundance analyses are that the subdwarfs comprising the Arcturus stream and AF06 stream identified as over-densities in phase space by

Arifanto & Fuchs (2006) have (i) a considerable spread in metallicity and (ii) relative abundance  $[X/Fe]$  identical to those of the Galactic thick disk. The metallicity spread excludes the hypothesis that either stream represents a dissolved open cluster. The high-degree of similarity between  $[X/Fe]$  at a given  $[Fe/H]$  for these streams and the field stars of the thick disk greatly strains a proposal that these streams represent the tidal debris of an accreted satellite galaxy. By exclusion, the likely origin of these streams is that they are the product of dynamical interactions within the Galaxy.

However, chemical identity with the thick disk and the non-similarity of their chemistry with the satellite galaxies within local group alone may not suffice to rule out the possibility of these streams being a result of disrupted satellites. It is still a matter of debate how perturbation can create streams with such a very high velocity drag and exhibit very tight abundance trends. It would be important to know from the models the extent of regions that get affected due to bar/spiral perturbations and their effect on the abundance trends of clumped stars in phase space. Astrometry from GAIA will provide unprecedented sample size as well as accuracy to map the Galaxy precisely which would decipher the Galaxy formation and evolution.

## ACKNOWLEDGMENTS

David Lambert thanks the Robert A. Welch Foundation for support through grant F-634. We thank Dr. Gajendra Pandey for useful comments. We also thank the referee for his/her remarks.

## REFERENCES

- Alonso A., Arribas S., Martinez-Roger C., 1996, *A&A*, 313, 873
- Antoja T., Valenzuela O., Pichardo B., Moreno E., Figueras F., Fernández D., 2009, *ApJ*, 700, L78-L82
- Arifanto M. I., Fuchs B., 2006, *A&A*, 449, 533
- Beers T. C. et al., 2000, *AJ*, 119, 2866
- Bensby T., Oey M. S., Feltzing S., Gustafsson B., 2007, *ApJ*, 655, L89
- Carney B. W., Latham D. W., Laird J. B., Aguilar L. A., 1994, *AJ*, 107, 2240
- Cayrel R., 1988, in Cayrel de Strobel G., Spite M., eds, *The Impact of Very High S/N Spectroscopy on Stellar Physics*. Kluwer Dordrecht, p.345
- Cutri R. M. et al., 2003., *Vizie Online Data Catalog*, II/246. Originally published in: Univ. of Massachusetts and Infrared Processing and Analysis Centre, IPAC/California Institute of technology.
- De Silva G. M., Freeman K. C., Bland-Hawthorn J., Asplund M., Bessell M. S., 2007, *AJ*, 133, 694
- De Silva G.M. et al., 2011, *MNRAS*, 415, 563
- De Silva G.M. et al., 2006, *AJ*, 131, 455
- Dehnen W., Binney J. J., 1998, *MNRAS*, 298, 387
- Demarque P., Woo J.-H., Kim Y.-C., Yi S. K., 2004, *ApJS*, 155, 667
- Eggen O. J., 1957, *The Observatory*, 77, 229
- Eggen O. J., 1971, *PASP*, 83, 271
- Eggen O. J., 1998, *AJ*, 115, 2397
- Freeman K., Bland-Hawthorn J., 2002, *ARA&A*, 40, 487
- Gratton R. G., Carretta E., Claudi R., Lucatello S., Barbieri M., 2003, *A&A*, 404, 187
- Hauck B., Mermilliod M., 1998, *A&AS*, 129, 431
- Helmi A., de Zeeuw P. T., 2000, *MNRAS*, 319, 657
- Helmi A. et al., 2006, *MNRAS*, 365, 1309
- Hinkle K., Wallace L., Valenti J., & Harmer D. (ed.) 2000, *Visible and Near Infrared Atlas of the Arcturus Spectrum 3727–9300 Å* (San Francisco, CA:ASP)
- Johnson D. R. H., Soderblom D. R., 1987, *AJ*, 93, 864
- Kharchenko N. V., 2001, *Kinematika i Fizika Nebesnykh Tel*, 17, 409
- Kirby E. N., 2011, in Koleva M., Prugniel P., Vauglin I., eds, *EAS Publications Series Vol. 48 of EAS Publications Series, The Elemental Abundance Distributions of Milky Way Satellite Galaxies*. pp 19–25
- Klement R., Fuchs B., Rix H.-W., 2008, *ApJ*, 685, 261
- Kurucz R.L., 1998, <http://kurucz.harvard.edu/> (online data)
- Minchev I. et al., 2010, *MNRAS*, 407, 2122
- Monaco L. et al., 2005, *A&A*, 441, 141
- Navarro J. F., Helmi A., Freeman K. C., 2004, *ApJ*, 601, L43
- Perryman M. A. C. et al., 1997, *A&A*, 323, L49
- Pompéia L. et al., 2011, *MNRAS*, 415, 1138
- Pancino E. et al., 2010, *A&A*, 524, A44
- Paunzen E. et al., 2010, *A&A*, 517, A32
- Ramírez I., Meléndez J., 2005, *ApJ*, 626, 446
- Reddy B. E., Lambert D. L., Allende Prieto C., 2006, *MNRAS*, 367, 1329
- Reddy B. E., Tomkin J., Lambert D. L., Allende Prieto C., 2003, *MNRAS*, 340, 304
- Schuster W. J., Nissen P. E., 1989, *A&A*, 221, 65
- Snedden C., 1973, PhD Thesis, Univ. of Texas, Austin
- Tolstoy E., Hill V., Tosi M., 2009, *ARA&A*, 47, 371
- Tull R. G., MacQueen P. J., Sneden C., Lambert D. L., 1995, *PASP*, 107, 251
- van Leeuwen F., 2007, *A&A*, 474, 653
- Venn K. A. et al., 2004, *AJ*, 128, 1177
- Williams M. E. K., Freeman K. C., Helmi A., RAVE Collaboration 2009, in J. Andersen, J. Bland-Hawthorn, & B. Nordström ed., *IAU Symposium Vol. 254 of IAU Symposium, The Arcturus Moving Group: Its Place in the Galaxy*. pp 139–144

**Table 1.** The atmospheric parameters - Photometry & Spectroscopy

Star	Photometry				Spectroscopy				
	(T <sub>eff</sub> ) <sub>V-K</sub> K	(T <sub>eff</sub> ) <sub>b-y</sub> K	log <i>g</i> ± error cm s <sup>-1</sup>	([M/H]) <sub>b-y</sub> dex	T <sub>eff</sub> K	log <i>g</i> cm s <sup>-1</sup>	([Fe/H]) <sub>model</sub> dex	ξ <sub>t</sub> km s <sup>-1</sup>	N
Arcturus stream									
HIP105888	5798	5665	4.05 ± 0.05	-0.81	5790	4.30	-0.55	1.08	(42,7)
HIP36710	5301	...	...	...	5340	4.63	-0.45	0.48	(46,6)
HIP77637	5478	5550	4.31 ± 0.08	-0.94	5580	3.73	-0.85	0.90	(30,7)
G103-53	5435	5340	4.16 ± 0.09	-0.66	5290	4.40	-0.65	0.52	(42,5)
G72-12	5041	5094	...	-0.27	5060	4.64	-0.40	0.67	(43,5)
G4-2	5258	5238	...	-0.61	5160	4.64	-0.70	0.48	(37,4)
HIP53070	5962	5719	4.23 ± 0.04	-1.30	...	...	-1.40	1.36	(4,3)
G204-30	5610	...	...	...	5550	4.42	-0.80	0.69	(27,5)
G139-49	5331	...	...	...	5380	4.12	-0.75	0.47	(30,5)
G241-7	5446	...	...	...	5320	4.00	-0.95	0.91	(25,4)
HIP40613	5723	5670	4.16 ± 0.03	-0.64	5670	4.02	-0.55	0.90	(45,6)
G42-34	4858	...	...	...	4920	4.22	-0.60	0.44	(47,4)
HIP36491	5741	5681	4.41 ± 0.05	-0.96	5760	4.20	-0.85	1.10	(25,6)
HIP94931	4964	5118	4.56 ± 0.01	-0.35	5120	4.58	-0.40	0.55	(48,6)
HIP74033	5647	5574	4.02 ± 0.04	-0.92	5690	4.04	-0.70	1.06	(42,7)
G5-1	5562	...	4.37 ± 0.08	...	5470	4.25	-1.05	0.45	(24,5)
G102-44	5253	...	...	...	5260	4.43	-0.63	0.44	(45,5)
HIP58253	5359	5351	...	-0.37	5280	4.38	-0.35	0.52	(41,4)
AF06 stream									
G67-40	5473	5326	...	-0.36	5370	4.42	-0.35	0.94	(48,6)
HIP9080	5078	...	...	...	5250	4.45	-0.25	0.53	(51,7)
G66-51	5420	...	...	...	5320	4.58	-0.80	0.79	(40,5)
G106-8	5799	...	4.13 ± 0.10	...	5780	4.23	-0.40	1.00	(38,8)
HIP10652	5607	5499	4.35 ± 0.03	-0.74	5580	4.42	-0.60	1.02	(38,5)
HIP22020	5610	...	4.12 ± 0.08	...	5690	4.15	-0.20	0.95	(51,8)
HIP26452	5837	...	...	...	5830	4.14	-0.68	0.70	(28,6)
HIP31740	5293	5436	4.31 ± 0.12	-0.32	5430	4.45	-0.35	0.62	(44,7)
HIP102923	4850	4933	4.61 ± 0.04	-0.19	4950	4.50	-0.25	0.69	(49,6)
G146-76	5170	...	...	...	5090	2.67	-1.60	0.82	(16,5)
HIP34642	5775	...	4.07 ± 0.05	...	5800	4.07	-0.40	1.00	(41,8)
G10-12	4957	...	...	...	5120	3.98	-0.45	0.84	(50,7)
HIP17147	5741	5722	4.22 ± 0.03	-0.83	5700	4.23	-0.85	0.71	(37,6)
HIP24030	5915	5697	4.16 ± 0.11	-1.06	5730	4.20	-1.05	1.16	(15,6)
HIP11952	6029	5785	4.24 ± 0.10	-1.57	...	...	...	1.38	(4,4)
HIP29814	5160	5217	4.48 ± 0.01	-0.37	5230	4.48	-0.40	0.75	(51,6)
G197-45	5176	...	...	...	5250	4.02	-0.60	0.85	(38,6)
HIP104913	5355	...	4.40 ± 0.02	...	5380	4.48	-0.03	0.80	(51,8)
G192-21	5790	5513	4.32 ± 0.10	-1.23	5820	4.20	-0.50	0.88	(36,6)
G69-21	5562	5500	...	-0.30	5620	4.29	-0.20	1.07	(48,7)
G68-10	5680	5589	4.36 ± 0.06	-0.57	5570	4.22	-0.50	0.73	(47,6)
G30-46	5076	...	...	...	5150	4.65	+0.15	0.68	(48,6)
HIP16169	5638	5575	4.34 ± 0.02	-0.56	5690	4.56	-0.48	1.10	(38,7)
G6-16	5786	5655	4.16 ± 0.10	-0.19	5800	4.30	-0.05	1.10	(48,8)
G78-41	5411	5494	4.37 ± 0.12	-0.38	5480	4.40	-0.40	0.74	(50,6)
G25-5	5487	5508	...	-0.36	5560	4.50	-0.35	0.93	(50,7)

**Table 2.** The Abundance ratios ( $[X/Fe]$ ) of the programme stars

Star	[FeI/H]	[O/Fe]	[Na/Fe]	[Mg/Fe]	[Al/Fe]	[Si/Fe]	[Ca/Fe]	[Sc/Fe]	[Ti/Fe]	[V/Fe]
Arcturus stream										
HIP105888	-0.56	0.58	0.10	0.25	0.20	0.16	0.12	0.17	0.24	0.08
HIP36710	-0.42	0.32	0.03	0.02	0.16	0.10	0.10	0.16	0.23	0.18
HIP77637	-0.82	0.69	-0.04	0.38	0.17	0.22	0.17	-0.09	0.15	-0.06
G103-53	-0.65	0.61	0.00	0.03	0.18	0.19	0.17	0.11	0.17	0.07
G72-12	-0.37	0.29	0.05	-0.01	0.12	0.14	0.01	0.16	0.13	0.21
G4-2	-0.70	0.38	-0.07	0.10	0.13	0.17	0.06	0.21	0.16	0.06
HIP53070	-1.40	0.84	...	...	...	...	0.27	...	...	...
G204-30	-0.81	0.60	0.11	0.30	0.19	0.22	0.19	0.11	0.24	0.07
G139-49	-0.75	0.69	-0.18	0.37	0.22	0.09	0.12	0.03	0.12	-0.18
G241-7	-0.94	0.92	0.22	0.51	0.20	0.18	0.30	0.00	0.28	-0.01
HIP40613	-0.54	0.61	0.09	0.37	0.27	0.16	0.17	0.03	0.23	0.01
G42-34	-0.60	0.26	0.03	0.09	0.16	-0.05	0.24	0.03	0.29	0.24
HIP36491	-0.86	0.56	0.11	0.43	0.27	0.19	0.19	0.12	0.19	—
HIP94931	-0.42	0.39	-0.01	0.12	0.14	0.11	0.10	0.18	0.21	0.23
HIP74033	-0.70	0.60	0.09	0.35	0.20	0.16	0.13	0.11	0.19	-0.03
G5-1	-1.04	0.62	-0.05	0.31	0.30	0.00	0.11	-0.03	0.19	-0.20
G102-44	-0.61	0.55	-0.03	0.03	0.17	0.08	0.16	-0.06	0.25	0.03
HIP58253	-0.38	0.61	-0.08	0.09	0.16	0.19	0.12	-0.05	0.15	0.18
AF06 stream										
G67-40	-0.38	0.37	0.08	0.21	0.22	0.18	0.16	0.08	0.21	0.22
HIP9080	-0.17	0.24	-0.03	0.08	0.04	0.03	0.01	-0.00	0.13	0.14
G66-51	-0.80	0.46	-0.01	0.27	0.21	0.14	0.21	0.03	0.29	0.18
G106-8	-0.41	0.42	0.08	0.28	0.16	0.15	0.13	0.09	0.21	0.11
HIP10652	-0.59	0.55	0.09	0.29	0.30	0.22	0.22	0.04	0.25	0.06
HIP22020	-0.22	0.36	0.01	0.21	0.21	0.14	0.10	0.09	0.22	0.01
HIP26452	-0.70	0.46	0.15	0.23	0.20	0.11	0.11	-0.05	0.16	0.02
HIP31740	-0.36	0.47	0.10	0.13	0.20	0.16	0.15	0.19	0.27	0.14
HIC102923	-0.29	0.32	0.14	0.11	0.06	0.11	0.12	0.16	0.29	0.47
G146-76	-1.59	0.86	...	0.28	...	0.31	0.12	-0.20	-0.01	...
HIP34642	-0.42	0.38	0.03	0.25	0.20	0.11	0.10	0.10	0.17	0.09
G10-12	-0.43	0.55	0.07	0.25	0.22	0.19	0.18	0.20	0.30	0.18
HIP17147	-0.86	0.75	0.08	0.42	0.28	0.22	0.22	0.08	0.23	-0.03
HIP24030	-1.07	0.73	0.06	0.37	0.27	0.24	0.24	-0.07	0.26	...
HIP11952	-1.69	1.25	...	...	...	...	0.33	...	...	...
HIP29814	-0.40	0.36	0.02	0.04	0.16	0.11	0.12	0.08	0.20	0.16
G197-45	-0.58	0.48	0.11	0.11	0.24	0.16	0.24	-0.10	0.24	0.10
HIC104913	-0.02	0.16	-0.05	0.09	-0.02	0.00	-0.05	0.08	0.02	0.04
G192-21	-0.50	0.49	0.11	0.30	0.19	0.07	0.15	0.06	0.26	0.10
G69-21	-0.22	0.27	0.01	0.12	0.11	0.04	0.04	-0.00	0.08	0.04
G68-10	-0.50	0.56	0.08	0.14	0.21	0.14	0.19	0.01	0.25	0.03
G30-46	+0.22	-0.03	-0.09	-0.10	-0.09	-0.05	-0.13	0.01	0.11	0.22
HIP16169	-0.44	0.49	0.05	0.31	0.21	0.17	0.11	0.16	0.20	0.09
G6-16	-0.02	0.09	-0.08	0.07	0.02	-0.03	-0.03	0.01	0.03	-0.03
G78-41	-0.40	0.55	0.04	0.09	0.20	0.16	0.11	0.10	0.25	0.11
G25-5	-0.32	0.35	0.12	0.03	0.18	0.14	0.11	0.11	0.23	0.16



**Table 3.** The Abundance ratios ( $[X/Fe]$ ) of the programme stars

Star	[CrI/Fe]	[CrII/Fe]	[Mn/Fe]	[Co/Fe]	[Ni/Fe]	[Cu/Fe]	[Zn/Fe]	[Y/Fe]	[Ba/Fe]	[Ce/Fe]	[Nd/Fe]	[Eu/Fe]
Arcturus stream												
HIP105888	-0.10	0.02	-0.34	0.13	-0.01	-0.05	0.30	0.02	-0.17	-0.02	0.16	0.36
HIP36710	-0.17	-0.04	-0.28	0.09	-0.04	0.07	0.21	-0.08	-0.22	0.15	...	0.41
HIP77637	-0.17	-0.06	-0.37	-0.01	-0.09	-0.20	0.26	0.09	0.01	-0.11	0.18	0.21
G103-53	-0.14	-0.10	-0.35	0.16	-0.05	0.13	0.26	-0.11	-0.19	0.14	0.26	0.10
G72-12	-0.11	-0.04	-0.24	0.10	-0.06	0.09	0.17	-0.01	-0.19	0.10	0.38	0.16
G4-2	-0.14	0.04	-0.31	0.09	-0.07	0.06	0.12	-0.15	-0.24	...	...	0.49
HIP53070	...	...	...	...	-0.06	...	0.12	0.19	0.03	...	...	...
G204-30	-0.17	...	-0.27	0.08	0.05	-0.08	0.14	0.05	-0.09	...	...	0.37
G139-49	-0.14	...	-0.37	0.05	-0.14	0.05	0.36	-0.15	-0.15	...	...	...
G241-7	-0.05	0.06	-0.48	0.07	0.01	0.01	0.43	0.05	-0.20	0.02	...	...
HIP40613	-0.18	0.00	-0.32	0.06	-0.04	-0.01	0.28	-0.07	-0.15	-0.26	0.03	0.24
G42-34	-0.11	...	-0.31	0.21	-0.10	0.16	0.02	-0.14	-0.23	0.33	0.05	0.47
HIP36491	-0.14	-0.06	-0.37	0.24	0.02	-0.12	0.20	-0.03	-0.17	0.15	0.46	0.34
HIP94931	-0.14	0.04	-0.20	0.06	-0.05	0.17	0.16	0.05	-0.21	0.17	0.16	0.43
HIP74033	-0.12	0.01	-0.30	0.10	-0.03	-0.02	0.32	0.11	-0.08	-0.04	0.16	0.33
G5-1	-0.18	-0.05	-0.43	0.07	-0.07	-0.40	0.08	-0.08	-0.22	0.13	...	0.29
G102-44	-0.10	0.02	-0.35	0.04	-0.07	-0.05	0.20	-0.09	-0.14	0.11	0.40	-0.01
HIP58253	-0.14	-0.01	-0.31	0.23	-0.00	0.01	0.13	-0.02	-0.09	...	...	0.13
AF06 stream												
G67-40	-0.11	-0.06	-0.28	0.08	0.04	0.14	0.15	-0.02	-0.23	0.17	...	0.36
HIP9080	-0.07	-0.06	-0.18	0.03	-0.02	0.23	0.08	0.07	-0.10	0.29	0.22	-0.01
G66-51	-0.02	...	-0.26	0.12	-0.02	0.05	0.05	0.08	-0.17	0.25	...	...
G106-8	-0.11	-0.04	-0.25	0.13	0.00	0.06	0.20	-0.07	-0.08	0.14	0.12	0.18
HIP10652	-0.07	-0.01	-0.30	0.08	0.07	0.05	0.12	0.01	-0.20	0.03	0.22	0.22
HIP22020	-0.03	0.02	-0.23	0.12	0.03	0.16	0.21	-0.05	-0.07	0.04	0.17	0.14
HIP26452	-0.09	0.01	-0.29	-0.04	-0.02	-0.19	0.14	-0.07	-0.05	0.22	0.48	0.09
HIP31740	-0.05	0.03	-0.26	0.04	0.04	0.21	0.25	0.07	-0.13	0.02	0.15	0.45
HIC102923	-0.02	0.01	-0.08	0.17	0.02	0.27	0.22	-0.11	-0.21	0.19	...	0.39
G146-76	-0.25	...	-0.56	...	-0.06	...	0.02	-0.23	0.05	...	...	0.23
HIP34642	-0.10	-0.06	-0.19	0.16	0.05	0.07	0.16	-0.04	0.00	-0.09	0.28	0.22
G10-12	-0.05	0.10	-0.26	0.15	0.05	0.17	0.25	0.06	-0.12	-0.01	0.24	0.41
HIP17147	-0.12	0.02	-0.41	0.08	0.01	-0.18	0.27	0.14	0.09	0.03	0.10	0.30
HIP24030	-0.03	...	-0.42	0.12	-0.01	-0.26	0.28	0.01	-0.03	...	...	-0.02
HIP11952	...	...	...	...	...	...	0.21	0.10	-0.15	...	...	...
HIP29814	-0.06	-0.20	-0.18	0.08	0.01	0.15	0.19	-0.05	-0.14	0.18	0.22	...
G197-45	0.03	0.02	-0.26	-0.03	0.02	0.15	0.09	-0.23	-0.28	0.14	...	0.10
HIP104913	-0.14	-0.13	-0.17	0.00	-0.06	0.13	0.10	-0.03	-0.11	0.16	0.27	0.18
G192-21	-0.08	-0.17	-0.38	0.12	0.05	0.10	0.15	-0.03	-0.08	...	...	0.12
G69-21	-0.08	0.01	-0.16	0.05	-0.01	0.13	0.09	-0.02	-0.08	0.09	0.29	0.15
G68-10	-0.08	-0.06	-0.31	0.11	0.02	0.05	0.29	-0.05	-0.16	-0.16	-0.07	-0.03
G30-46	-0.10	-0.03	-0.13	-0.02	-0.10	0.15	-0.08	-0.09	-0.26	0.08	0.12	0.07
HIP16169	-0.09	-0.02	-0.23	0.14	0.03	0.06	0.07	0.01	-0.19	0.16	0.04	0.07
G6-16	-0.04	0.03	-0.14	-0.10	-0.05	0.11	-0.02	-0.12	-0.07	0.00	0.10	-0.01
G78-41	-0.09	-0.03	-0.29	0.08	0.01	0.21	0.20	-0.04	-0.18	0.07	0.18	0.28
G25-5	-0.04	0.03	-0.19	0.09	0.03	0.12	0.12	-0.04	-0.14	0.05	0.36	0.29

**Table 4.** Error Analysis of the star HIP40613

Quantity	N	$\Delta T_{\text{eff}}$ $\pm 50$ K	$\Delta \log g$ $\pm 0.2$ dex	$\Delta \xi_t$ $\pm 0.2$ km/s	$\Delta [M/H]$ $\pm 0.1$ dex	$\Delta W_\lambda$ $\pm 2\text{m}\text{\AA}$	$\sigma_{\text{model}}$
$\Delta [\text{OI}/\text{Fe}]$	3	$\pm 0.05$	$\pm 0.04$	$\pm 0.01$	$\pm 0.01$	$\pm 0.02$	$\pm 0.07$
$\Delta [\text{NaI}/\text{Fe}]$	2	$\pm 0.03$	$\pm 0.01$	$\pm 0.00$	$\pm 0.00$	$\pm 0.03$	$\pm 0.04$
$\Delta [\text{MgI}/\text{Fe}]$	2	$\pm 0.03$	$\pm 0.03$	$\pm 0.02$	$\pm 0.00$	$\pm 0.02$	$\pm 0.05$
$\Delta [\text{AlI}/\text{Fe}]$	5	$\pm 0.02$	$\pm 0.03$	$\pm 0.01$	$\pm 0.00$	$\pm 0.01$	$\pm 0.04$
$\Delta [\text{SiI}/\text{Fe}]$	7	$\pm 0.01$	$\pm 0.01$	$\pm 0.01$	$\pm 0.00$	$\pm 0.01$	$\pm 0.02$
$\Delta [\text{CaI}/\text{Fe}]$	5	$\pm 0.04$	$\pm 0.03$	$\pm 0.03$	$\pm 0.00$	$\pm 0.01$	$\pm 0.06$
$\Delta [\text{ScII}/\text{Fe}]$	3	$\pm 0.01$	$\pm 0.08$	$\pm 0.02$	$\pm 0.02$	$\pm 0.03$	$\pm 0.09$
$\Delta [\text{TiI}/\text{Fe}]$	7	$\pm 0.05$	$\pm 0.02$	$\pm 0.02$	$\pm 0.00$	$\pm 0.01$	$\pm 0.06$
$\Delta [\text{VI}/\text{Fe}]$	5	$\pm 0.06$	$\pm 0.01$	$\pm 0.00$	$\pm 0.00$	$\pm 0.03$	$\pm 0.07$
$\Delta [\text{CrI}/\text{Fe}]$	4	$\pm 0.05$	$\pm 0.01$	$\pm 0.01$	$\pm 0.00$	$\pm 0.02$	$\pm 0.06$
$\Delta [\text{CrII}/\text{Fe}]$	1	$\pm 0.02$	$\pm 0.08$	$\pm 0.02$	$\pm 0.02$	$\pm 0.08$	$\pm 0.12$
$\Delta [\text{MnI}/\text{Fe}]$	3	$\pm 0.06$	$\pm 0.01$	$\pm 0.01$	$\pm 0.00$	$\pm 0.01$	$\pm 0.06$
$\Delta [\text{FeI}/\text{H}]$	45	$\pm 0.04$	$\pm 0.01$	$\pm 0.03$	$\pm 0.01$	$\pm 0.00$	$\pm 0.05$
$\Delta [\text{FeII}/\text{H}]$	6	$\pm 0.02$	$\pm 0.08$	$\pm 0.04$	$\pm 0.02$	$\pm 0.01$	$\pm 0.09$
$\Delta [\text{CoI}/\text{Fe}]$	3	$\pm 0.04$	$\pm 0.00$	$\pm 0.01$	$\pm 0.00$	$\pm 0.02$	$\pm 0.05$
$\Delta [\text{NiI}/\text{Fe}]$	16	$\pm 0.03$	$\pm 0.01$	$\pm 0.02$	$\pm 0.00$	$\pm 0.01$	$\pm 0.04$
$\Delta [\text{CuI}/\text{Fe}]$	3	$\pm 0.04$	$\pm 0.02$	$\pm 0.04$	$\pm 0.01$	$\pm 0.04$	$\pm 0.07$
$\Delta [\text{ZnI}/\text{Fe}]$	2	$\pm 0.01$	$\pm 0.02$	$\pm 0.05$	$\pm 0.02$	$\pm 0.03$	$\pm 0.07$
$\Delta [\text{YII}/\text{Fe}]$	4	$\pm 0.01$	$\pm 0.08$	$\pm 0.04$	$\pm 0.02$	$\pm 0.02$	$\pm 0.09$
$\Delta [\text{BaII}/\text{Fe}]$	3	$\pm 0.02$	$\pm 0.03$	$\pm 0.12$	$\pm 0.03$	$\pm 0.01$	$\pm 0.13$
$\Delta [\text{CeII}/\text{Fe}]$	1	$\pm 0.01$	$\pm 0.08$	$\pm 0.01$	$\pm 0.03$	$\pm 0.13$	$\pm 0.16$
$\Delta [\text{NdII}/\text{Fe}]$	1	$\pm 0.02$	$\pm 0.09$	$\pm 0.01$	$\pm 0.03$	$\pm 0.16$	$\pm 0.19$
$\Delta [\text{EuII}/\text{Fe}]$	2	$\pm 0.01$	$\pm 0.09$	$\pm 0.01$	$\pm 0.03$	$\pm 0.07$	$\pm 0.12$

**Table 5.** Comparison of current study with the Reddy et al. (2006) sample for common stars

Quantity	HIP40613	HIP74033	HIP9080	HIP10652	HIP22020	HIP24030	HIP34642	Mean (dex)
$\Delta T_{\text{eff}}$	0.00	116.00	88.00	81.00	86.00	-8.00	53.00	$59 \pm 47$
$\Delta \log g$	-0.14	0.09	-0.20	-0.16	-0.12	-0.44	-0.07	$-0.15 \pm 0.16$
$\Delta [\text{FeI}/\text{H}]$	0.08	0.15	0.20	0.08	0.13	-0.07	0.02	$0.08 \pm 0.09$
$\Delta [\text{O}/\text{Fe}]$	-0.08	-0.20	-0.33	-0.15	-0.15	0.04	-0.06	$-0.13 \pm 0.12$
$\Delta [\text{Na}/\text{Fe}]$	-0.06	-0.07	-0.02	0.02	-0.09	-0.07	-0.01	$-0.04 \pm 0.04$
$\Delta [\text{Mg}/\text{Fe}]$	-0.02	-0.06	-0.06	0.05	-0.03	0.07	0.15	$0.01 \pm 0.08$
$\Delta [\text{Al}/\text{Fe}]$	-0.01	...	-0.09	0.05	-0.04	0.08	-0.01	$0.00 \pm 0.06$
$\Delta [\text{Si}/\text{Fe}]$	-0.05	-0.11	-0.12	0.06	-0.05	0.00	0.00	$-0.04 \pm 0.06$
$\Delta [\text{Ca}/\text{Fe}]$	0.02	-0.12	...	0.09	-0.01	0.12	0.06	$0.03 \pm 0.09$
$\Delta [\text{Sc}/\text{Fe}]$	-0.13	-0.02	-0.21	-0.15	-0.03	-0.15	0.12	$-0.08 \pm 0.11$
$\Delta [\text{Ti}/\text{Fe}]$	0.04	-0.05	0.08	0.12	0.05	0.07	0.11	$0.06 \pm 0.06$
$\Delta [\text{V}/\text{Fe}]$	0.00	-0.14	0.08	0.07	-0.01	...	0.11	$0.02 \pm 0.09$
$\Delta [\text{Cr}/\text{Fe}]$	-0.15	...	-0.02	-0.06	0.00	0.03	-0.06	$-0.04 \pm 0.06$
$\Delta [\text{Mn}/\text{Fe}]$	-0.01	0.05	-0.14	0.03	0.00	0.12	0.08	$0.02 \pm 0.08$
$\Delta [\text{Co}/\text{Fe}]$	-0.03	-0.10	-0.07	0.02	0.03	0.10	0.14	$0.01 \pm 0.09$
$\Delta [\text{Ni}/\text{Fe}]$	0.00	-0.06	-0.13	0.05	0.04	-0.04	0.07	$-0.01 \pm 0.07$
$\Delta [\text{Zn}/\text{Fe}]$	0.18	0.14	0.06	0.02	0.10	0.15	0.20	$0.12 \pm 0.07$
$\Delta [\text{Y}/\text{Fe}]$	-0.02	-0.06	0.35	0.08	0.08	-0.20	0.12	$0.05 \pm 0.17$
$\Delta [\text{Ba}/\text{Fe}]$	0.04	0.03	0.01	-0.11	-0.01	-0.04	...	$-0.01 \pm 0.06$
$\Delta [\text{Ce}/\text{Fe}]$	-0.11	-0.06	0.08	0.10	0.02	...	0.14	$0.03 \pm 0.10$
$\Delta [\text{Nd}/\text{Fe}]$	-0.04	-0.03	...	...	...	...	0.20	$0.04 \pm 0.14$
$\Delta [\text{Cu}/\text{Fe}]$	0.03	0.07	0.20	0.07	0.12	0.07	0.17	$0.10 \pm 0.06$
$\Delta [\text{Eu}/\text{Fe}]$	0.00	-0.01	-0.20	-0.17	-0.07	...	0.07	$-0.06 \pm 0.10$

**Table 6.** The kinematical parameters of the sample.

Star	$R_V$ km s <sup>-1</sup>	$U_{LSR} \pm 1\sigma$ km s <sup>-1</sup>	$V_{LSR} \pm 1\sigma$ km s <sup>-1</sup>	$W_{LSR} \pm 1\sigma$ km s <sup>-1</sup>	$R_m$ kpc	$e$	$Z_{max}$ kpc	Age Gyr	P %	$J_z$ kpc km s <sup>-1</sup>	$J_\perp$ kpc km s <sup>-1</sup>
Arcturus stream											
HIP105888	-84.3	-23.9 ± 0.7	-122.4 ± 4.8	-40.0 ± 6.5	5.42	0.57	0.35	10.8 <sup>+0.9</sup> <sub>-0.8</sub>	97 ± 0	-825	338
HIP36710	-70.8	+45.8 ± 1.3	-107.3 ± 6.9	+45.3 ± 7.0	5.82	0.51	0.42	...	97 ± 1	-965	388
HIP77637	-51.0	-26.9 ± 1.2	-134.0 ± 17.7	+15.8 ± 6.1	5.21	0.63	0.14	...	96 ± 0	-724	131
G103-53	+10.0	+10.0 ± 1.8	-125.4 ± 19.1	-55.4 ± 9.6	5.44	0.58	0.54	...	96 ± 3	-813	476
G72-12	-34.3	-13.7 ± 6.6	-118.7 ± 15.0	-62.9 ± 12.7	5.55	0.55	0.65	...	96 ± 2	-866	538
G4-2	+38.8	-11.1 ± 1.2	-117.2 ± 19.8	-76.0 ± 8.1	5.60	0.54	0.90	...	95 ± 4	-880	650
HIP53070	+65.8	-23.6 ± 0.71	-124.8 ± 4.84	+22.9 ± 2.1	5.41	0.59	0.19	...	95 ± 1	-811	194
G204-30	-69.7	+58.9 ± 11.5	-130.4 ± 12.0	+46.9 ± 10.7	5.43	0.62	0.44	...	95 ± 3	-763	399
G139-49	-94.1	-25.9 ± 5.5	-131.7 ± 11.8	-6.7 ± 1.9	5.24	0.62	0.06	...	95 ± 1	-742	57
G241-7	-113.6	-45.5 ± 14.1	-134.1 ± 5.3	-20.4 ± 1.5	5.34	0.64	0.16	...	95 ± 0	-729	175
HIP40613	+112.5	-31.6 ± 1.7	-139.0 ± 3.3	-32.7 ± 3.5	5.21	0.66	0.27	12.9 <sup>+0.5</sup> <sub>-0.3</sub>	95 ± 1	-692	279
G42-34	+36.9	+8.4 ± 2.7	-126.5 ± 17.6	-7.1 ± 6.5	5.37	0.59	0.08	...	94 ± 6	-799	60
HIP36491	+90.8	-47.7 ± 1.8	-118.9 ± 6.1	+1.2 ± 2.2	5.60	0.57	0.01	...	91 ± 4	-865	10
HIP94931	-121.4	+65.9 ± 2.7	-120.7 ± 1.2	-79.2 ± 1.8	5.70	0.58	0.95	13.4 <sup>+3.2</sup> <sub>-0.1</sub>	91 ± 1	-845	672
HIP74033	-59.8	-111.7 ± 7.5	-132.7 ± 11.5	+42.3 ± 7.2	5.83	0.68	0.40	12.0 <sup>+1.6</sup> <sub>-1.3</sub>	89 ± 5	-738	351
G5-1	-22.4	+44.8 ± 2.4	-125.7 ± 15.5	-85.7 ± 13.2	5.56	0.59	1.07	...	89 ± 8	-810	737
G102-44	-29.2	+73.6 ± 5.4	-130.5 ± 21.3	+88.1 ± 11.7	5.68	0.63	1.15	...	82 ± 14	-769	759
HIP58253	+29.3	-62.5 ± 7.5	-106.2 ± 10.8	-3.4 ± 4.2	5.89	0.52	0.08	...	80 ± 16	-969	34
AF06 stream											
G67-40	-29.2	-94.8 ± 15.3	-84.5 ± 10.2	-54.8 ± 12.2	6.61	0.48	0.57	...	97 ± 1	-1144	459
HIP9080	-10.2	-92.8 ± 20.9	-91.2 ± 17.9	+54.2 ± 7.7	6.49	0.49	0.57	...	97 ± 1	-1098	469
G66-51	-118.5	-86.1 ± 2.5	-79.8 ± 10.5	-66.9 ± 2.2	6.62	0.44	0.76	...	97 ± 0	-1183	571
G106-8	+49.4	-16.3 ± 2.5	-92.2 ± 11.0	+85.9 ± 13.4	6.12	0.42	1.05	14.0 <sup>+1</sup> <sub>-1.3</sub>	96 ± 2	-1097	737
HIP10652	-20.9	-78.2 ± 7.7	-79.1 ± 5.7	+84.7 ± 4.9	6.68	0.42	1.08	...	96 ± 1	-1201	726
HIP22020	+30.6	-74.3 ± 7.9	-85.6 ± 14.5	-52.9 ± 8.7	6.46	0.45	0.53	11.8 <sup>+1.2</sup> <sub>-2</sub>	96 ± 3	-1151	455
HIP26452	-35.8	+ 1.2 ± 4.6	-98.0 ± 10.3	+50.0 ± 6.7	5.91	0.45	0.47	...	96 ± 3	-1045	428
HIP31740	+86.2	-94.8 ± 4.3	-107.5 ± 21.5	+49.6 ± 2.7	6.20	0.56	0.50	...	96 ± 2	-964	423
HIP102923	-61.7	-12.2 ± 1.0	-92.0 ± 3.4	-52.6 ± 5.3	5.98	0.42	0.50	...	96 ± 2	-1084	446
G146-76	-113.7	+50.3 ± 1.5	-80.6 ± 8.6	-90.6 ± 1.0	6.46	0.39	1.16	...	96 ± 1	-1189	770
HIP34642	-28.1	-13.1 ± 5.4	-85.5 ± 9.4	-53.9 ± 5.6	6.19	0.39	0.52	10.6 <sup>+1.3</sup> <sub>-1.6</sub>	95 ± 4	-1154	463
G10-12	+133.0	-52.1 ± 6.5	-91.4 ± 4.8	+96.8 ± 3.8	6.24	0.43	1.29	...	94 ± 1	-1095	822
HIP17147	+120.0	-101.3 ± 0.9	-83.8 ± 1.2	-34.2 ± 1.0	6.70	0.48	0.31	...	88 ± 1	-1160	290
HIP24030	-15.9	+21.4 ± 1.2	-105.6 ± 23.5	+112.3 ± 20.5	5.94	0.47	1.65	...	85 ± 16	-984	966
HIP11952	+24.0	+38.0 ± 6.47	-90.7 ± 15.3	-30.7 ± 2.9	6.11	0.43	0.29	...	72 ± 27	-1106	267
HIP29814	+22.1	-43.2 ± 2.1	-92.8 ± 6.0	-20.9 ± 2.0	6.08	0.45	0.17	...	62 ± 13	-1087	179
G197-45	+22.8	-67.0 ± 10.4	-76.9 ± 13.2	+32.1 ± 1.2	6.55	0.40	0.29	...	61 ± 24	-1219	268
HIP104913	-64.5	-69.6 ± 5.4	-80.4 ± 1.8	+26.9 ± 1.9	6.47	0.42	0.23	11.9 <sup>+1.9</sup> <sub>-2.6</sub>	58 ± 6	-1184	228
G192-21	-18.6	+ 7.0 ± 3.2	-88.4 ± 13.1	+22.1 ± 3.0	6.08	0.41	0.18	11.2 <sup>+2.1</sup> <sub>-2.9</sub>	47 ± 28	-1125	189
G69-21	-15.8	-87.8 ± 15.6	-80.9 ± 11.1	+ 3.2 ± 2.0	6.63	0.45	0.06	...	45 ± 24	-1182	33
G68-10	-40.6	-86.1 ± 8.6	-76.8 ± 4.6	-16.0 ± 4.4	6.67	0.43	0.14	13.2 <sup>+1.7</sup> <sub>-1.5</sub>	45 ± 11	-1213	133
G30-46	-22.9	-75.1 ± 13.4	-80.8 ± 10.6	-12.9 ± 5.5	6.50	0.43	0.13	...	42 ± 22	-1181	105
HIP16169	+63.3	-47.4 ± 1.0	-87.5 ± 3.6	-10.5 ± 1.4	6.20	0.42	0.09	12.85 <sup>+1.05</sup> <sub>-0.1</sub>	40 ± 7	-1131	88
G6-16	+25.6	-31.4 ± 3.0	-85.4 ± 14.3	-15.9 ± 1.9	6.21	0.40	0.13	11.0 <sup>+1.1</sup> <sub>-1.5</sub>	36 ± 27	-1154	135
G78-41	-10.3	-18.7 ± 5.7	-88.7 ± 13.3	-3.3 ± 2.3	6.11	0.41	0.03	...	32 ± 25	-1127	28
G25-5	-38.1	+44.2 ± 8.4	-85.0 ± 9.5	-2.4 ± 3.9	6.17	0.41	0.04	...	31 ± 17	-1143	23

**Table 7.** Mean elemental abundance ratios and dispersions

Element	Arcturus		AF06		Thick disk		$\sigma_{\text{model}}$
	Mean	$\sigma$	Mean	$\sigma$	Mean	$\sigma$	
[O/Fe]	0.54	0.13	0.48	0.08	0.60	0.12	0.07
[Na/Fe]	0.03	0.09	0.07	0.04	0.10	0.06	0.04
[Mg/Fe]	0.21	0.11	0.21	0.09	0.30	0.07	0.05
[Al/Fe]	0.18	0.04	0.21	0.03	0.26	0.08	0.04
[Si/Fe]	0.14	0.06	0.15	0.04	0.22	0.06	0.02
[Ca/Fe]	0.14	0.05	0.16	0.04	0.16	0.06	0.06
[Sc/Fe]	0.07	0.09	0.07	0.07	0.14	0.09	0.09
[TiI/Fe]	0.20	0.05	0.23	0.04	0.19	0.07	0.06
[V/Fe]	0.07	0.08	0.11	0.06	0.11	0.08	0.07
[CrI/Fe]	-0.13	0.03	-0.07	0.04	-0.03	0.04	0.06
[CrII/Fe]	-0.01	0.05	-0.03	0.08	...	...	0.12
[Mn/Fe]	-0.32	0.05	-0.27	0.05	-0.26	0.07	0.06
[Co/Fe]	0.10	0.07	0.09	0.05	0.10	0.05	0.05
[Ni/Fe]	-0.04	0.05	0.02	0.02	0.02	0.04	0.04
[Cu/Fe]	0.01	0.08	0.08	0.08	-0.02	0.07	0.07
[Zn/Fe]	0.22	0.09	0.17	0.07	0.12	0.06	0.07
[Y/Fe]	-0.03	0.08	-0.02	0.08	0.00	0.11	0.09
[Ba/Fe]	-0.15	0.06	-0.13	0.08	-0.14	0.09	0.13
[Ce/Fe]	0.06	0.15	0.08	0.11	0.06	0.13	0.16
[Nd/Fe]	0.22	0.14	0.19	0.14	0.20	0.16	0.19
[Eu/Fe]	0.29	0.15	0.22	0.13	0.36	0.12	0.12

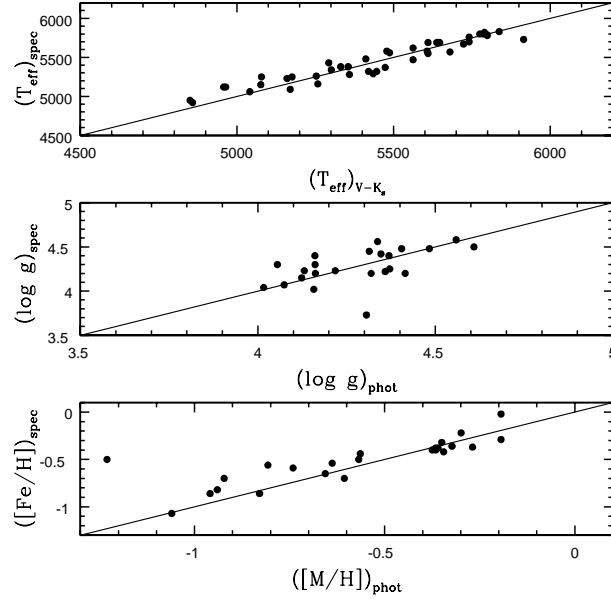


**Figure 1.** Comparison of atmospheric parameters derived using spectroscopy and photometry.

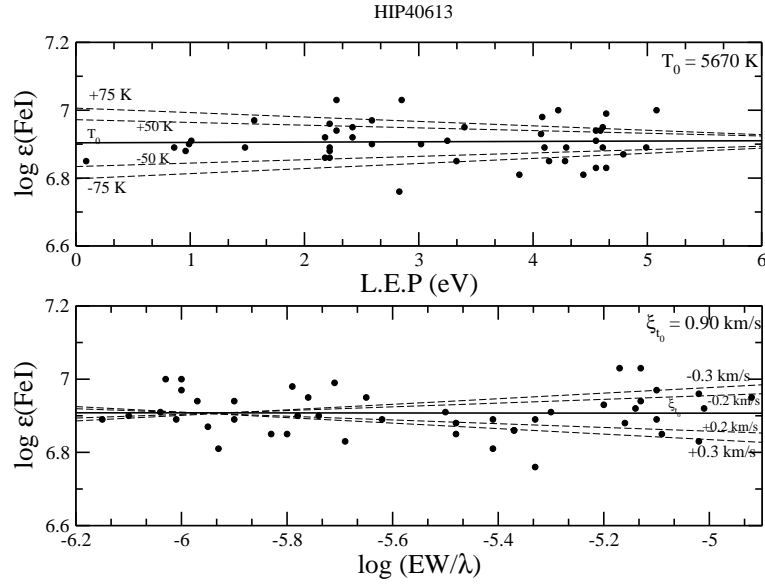


**Figure 2.** E

estimation of uncertainties in the  $T_{\text{eff}}$  (top) and  $\xi_t$  (bottom). The solid center line is for the best representative model parameter. Broken lines represent models with increasing or decreasing  $T_{\text{eff}}$  and  $\xi_t$  in steps of 25 K and 0.1 km s<sup>-1</sup>, respectively.

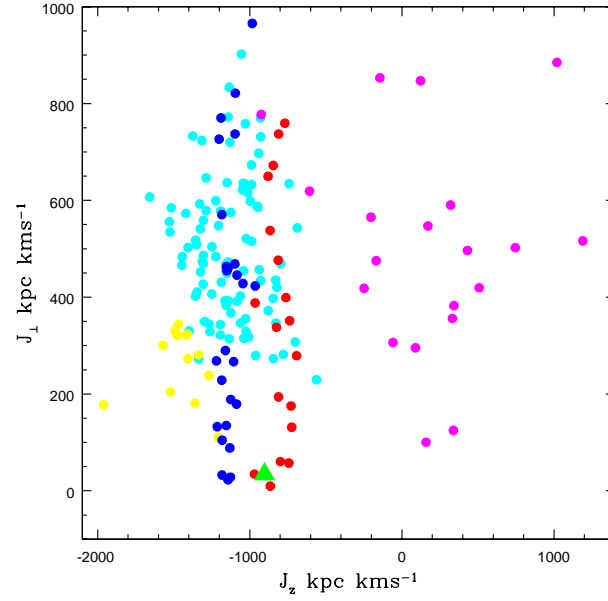


**Figure 3.** Stream stars are shown with members of halo, thick disk and thin disk stars taken from Reddy et al. (2006) in the angular momentum space:  $J_{\perp}$  versus  $J_z$ . Red : Arcturus stream, Blue : AF06 stream, Cyan : Thick disk, Yellow : Thin disk, Magenta : Halo, Green : Giant Arcturus. [Colour Online]

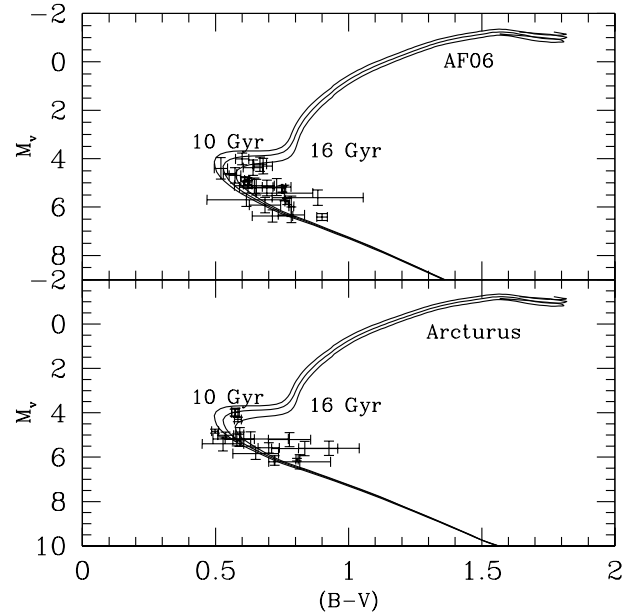


**Figure 4.** The colour-magnitude diagram for the Arcturus and AF06 stream.

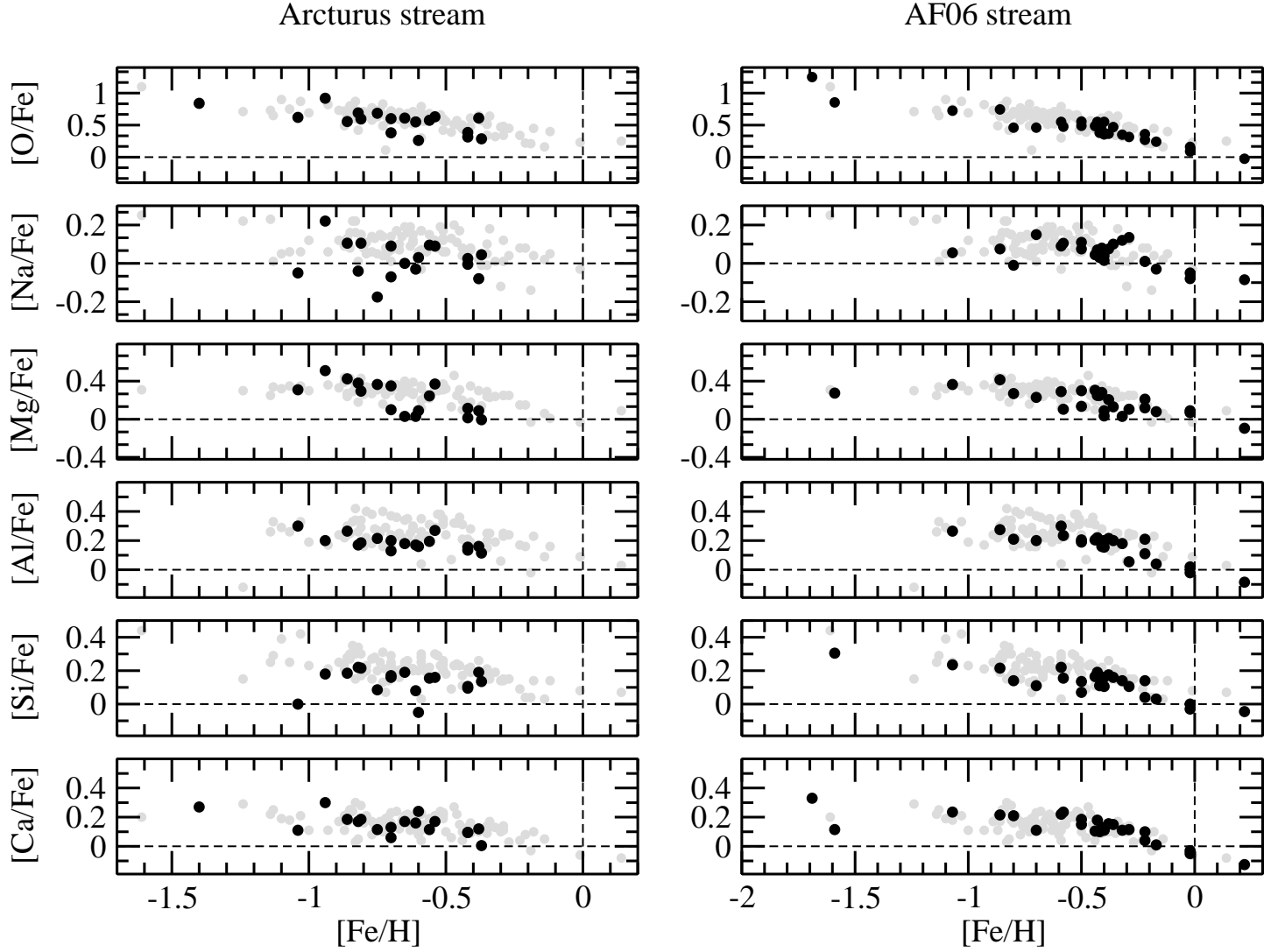


**Figure 5.** The abundance plots of elements - O, Na, Mg, Al, Si and Ca for the Arcturus stream (left column) and AF06 stream (right column). Grey symbols represent the field thick disk members from Reddy et al. (2006). [Colour Online]

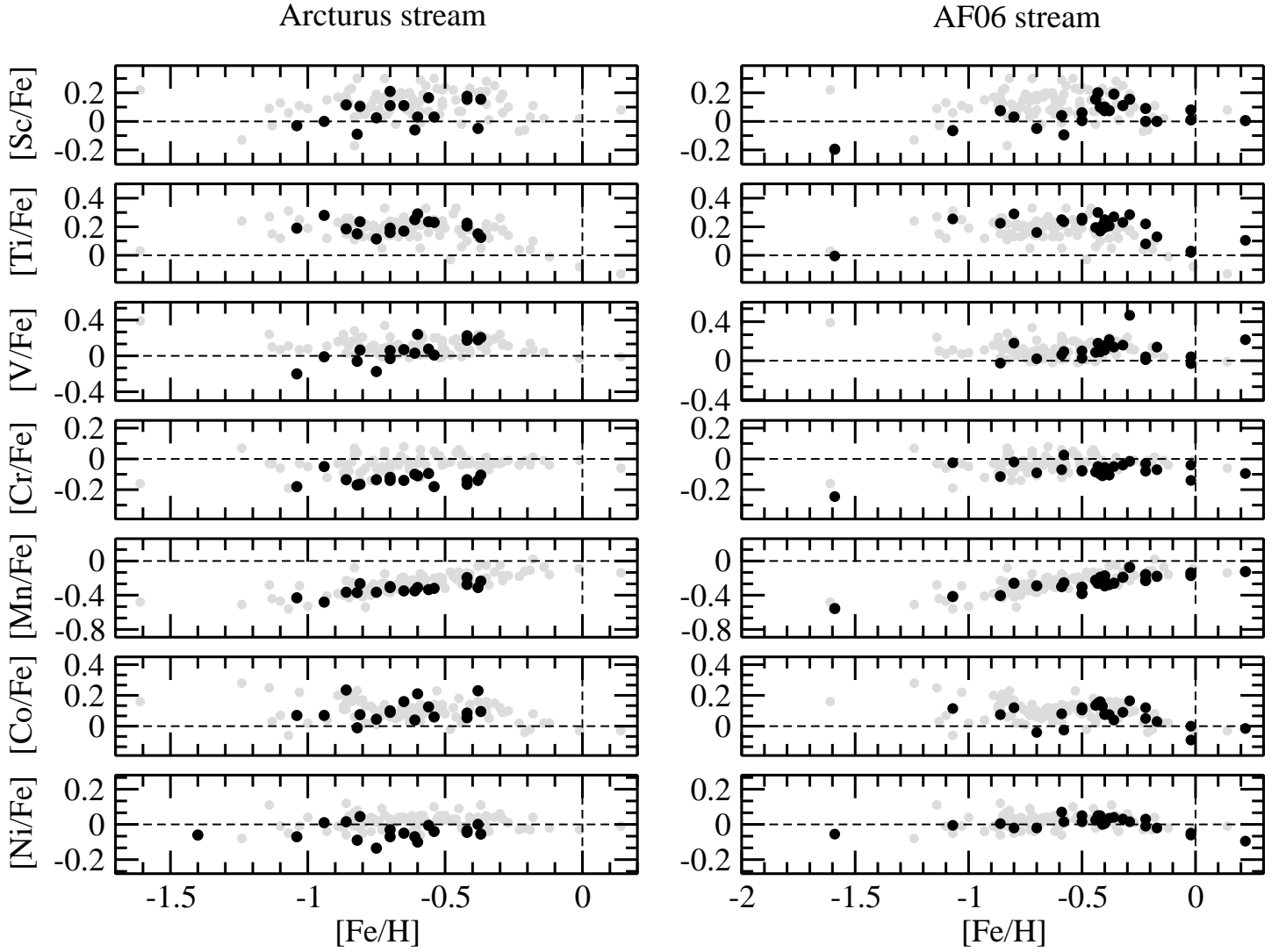


**Figure 6.** Same as Figure 4 but for the elements - Sc, Ti, V, Cr, Mn, Co and Ni. [Colour Online]



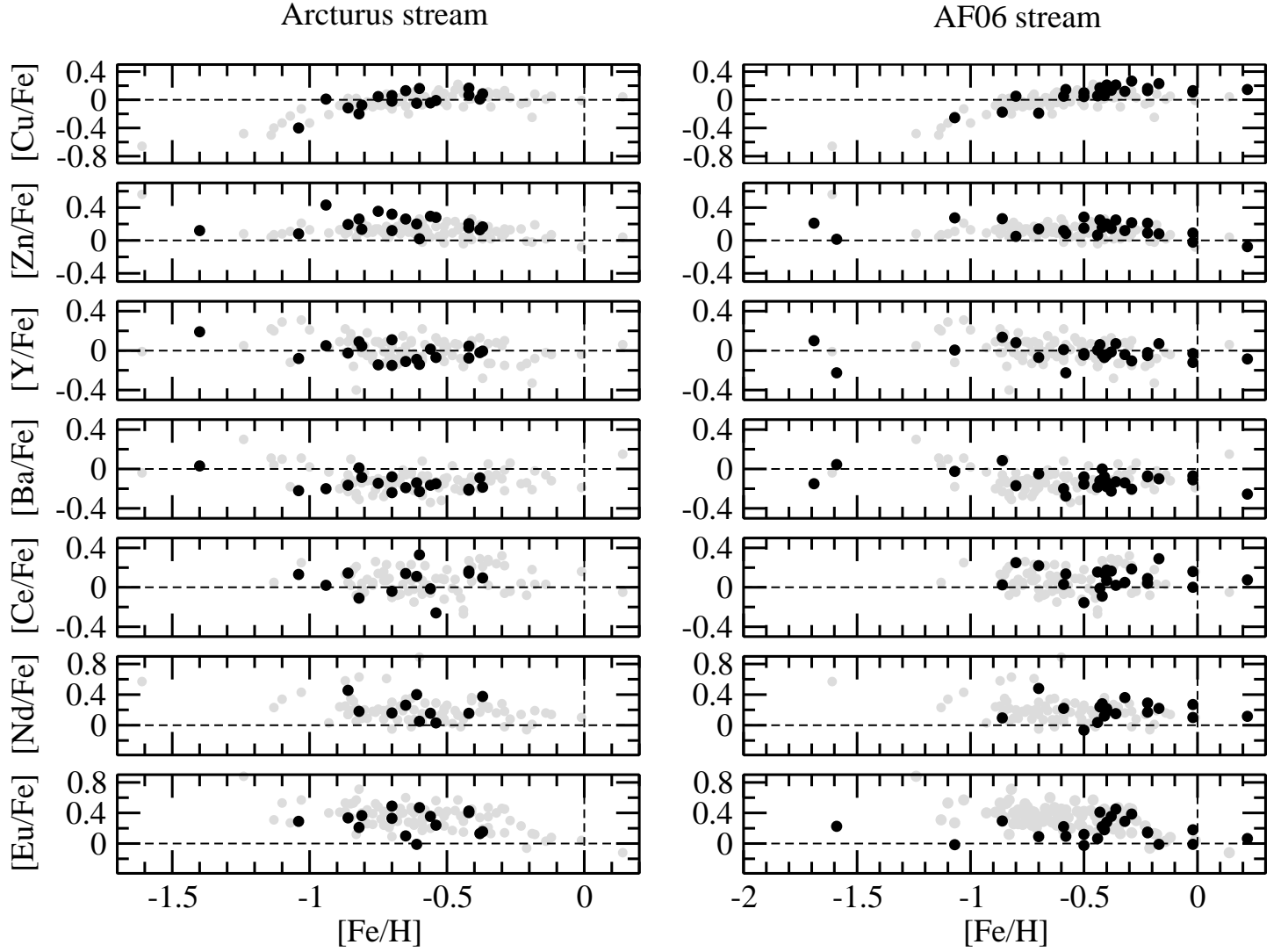


**Figure 7.** Same as Figure 4 but for the elements - Cu, Zn, Y, Ba, Ce, Nd and Eu. [Colour Online]

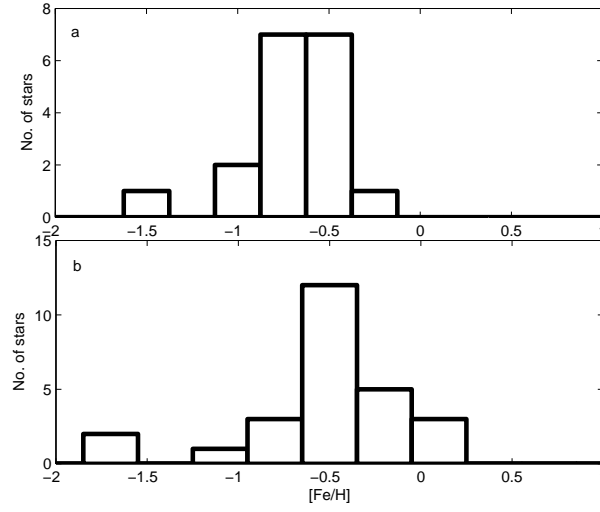


**Figure 8.** The metallicity distribution of a) the Arcturus stream, binsize = 0.25 dex and b) the AF06 stream, binsize = 0.3 dex.

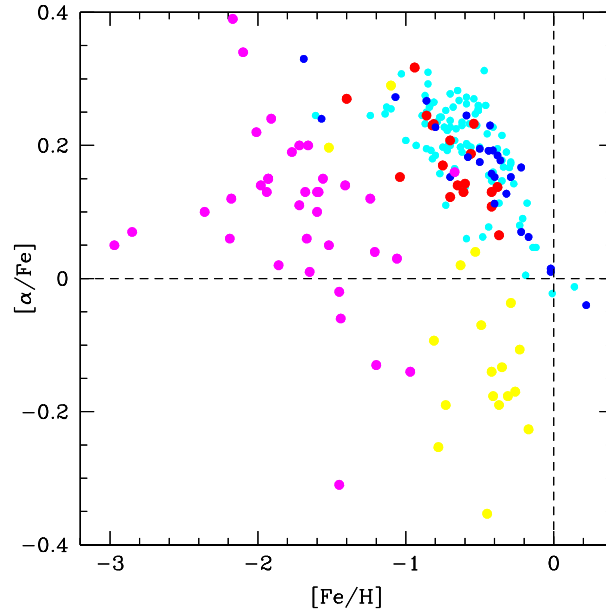


**Figure 9.** The  $[\alpha/\text{Fe}]$  versus  $[\text{Fe}/\text{H}]$  plot. Red : Arcturus stream, Blue : AF06 stream, Cyan : Thick disk, Magenta : dSph satellite galaxies (Draco, Sculptor, Sextans, Ursa Minor, Carina, Fornax, Leo I) from Venn et al (2004), yellow : Sgr dSph from Monaco et al. (2005) with  $[\alpha/\text{Fe}] = ([\text{Mg}/\text{Fe}] + [\text{Ca}/\text{Fe}] + [\text{Ti}/\text{Fe}])/3$ . [Colour Online]

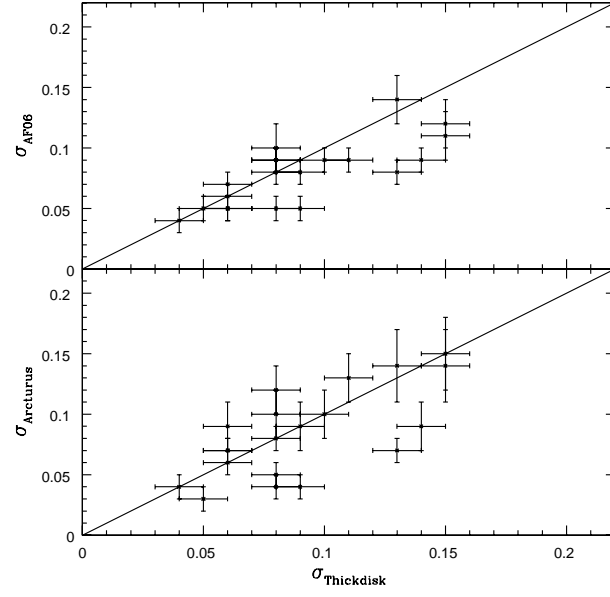


**Figure 10.** The dispersions in  $[X/\text{Fe}]$  of members of the Arcturus stream, the AF06 stream and the field thick disk sample